PHYSICAL REVIEW B **74**, 060406(R) (2006)

Origin of fourfold anisotropy in square lattices of circular ferromagnetic dots

G. N. Kakazei,[1,2] Yu. G. Pogorelov,[3] M. D. Costa,[4] T. Mewes,[5] P. E. Wigen,[2] P. C. Hammel,[2] V. O. Golub,[1] T. Okuno,[6] and V. Novosad[7]

[1]*Institute of Magnetism, National Academy of Sciences of Ukraine, 36b Vernadskogo boulevard, 03142 Kiev, Ukraine*
[2]*Department of Physics, The Ohio State University, 191 West Woodruff Avenue, Columbus, Ohio 43210, USA*
[3]*IFIMUP/Departamento de Física, Universidade do Porto, R. Campo Alegre, 687, Porto, 4169, Portugal*
[4]*CFP/Departmento de Física, Universidade do Porto, R. Campo Alegre, 687, Porto, 4169, Portugal*
[5]*MINT/Department of Physics and Astronomy, University of Alabama, Box 870209, Tuscaloosa, Alabama 35487, USA*
[6]*Institute for Chemical Research, Kyoto University, Kyoto 611-0011, Japan*
[7]*Materials Science Division, Argonne National Laboratory, Argonne, Illinois 60439, USA*

(Received 13 June 2006; revised manuscript received 28 July 2006; published 30 August 2006)

We discuss the fourfold anisotropy of the in-plane ferromagnetic resonance field H_r, found in a square lattice of circular Permalloy dots when the interdot distance a becomes comparable to the dot diameter d. The minimum H_r along the lattice $\langle 11 \rangle$ axes and the maximum along the $\langle 10 \rangle$ axes differ by ~ 50 Oe at $a/d=1.1$. This anisotropy, not expected in uniformly magnetized dots, is explained by a mechanism of nonuniform magnetization $\mathbf{m}(\mathbf{r})$ in a dot in response to dipolar forces in the patterned magnetic structure under strong enough applied field. It is well described by an iterative solution of a continuous variational procedure.

DOI: 10.1103/PhysRevB.74.060406 PACS number(s): 75.10.Hk, 75.30.Gw, 75.70.Cn, 76.50.+g

Magnetic nanostructures are of increasing interest for technological applications, such as patterned recording media[1] or magnetic random access memories.[2] One of the most important issues for understanding their collective behavior is the effect of long-range dipolar interactions between the dots.[3] For the single-domain magnetic state of a dot, the simplest approximation is that dots are uniformly magnetized and interactions only define the relative orientation of their magnetic moments.[4] If so, the system of dipolar coupled dots in a square lattice should be magnetically isotropic.

However, in all known experimental studies of closely packed arrays of circular dots, a fourfold anisotropy (FFA) was found, by either Brillouin light scattering,[5] ferromagnetic resonance[6] (FMR), or magnetization measurements (from hysteresis loops).[7,8] To explain this effect under weak enough applied field, a mechanism of vortex displacements was suggested[7] and described in a model of two competing domains.[9] But it is important to note that the FFA exists also in almost saturated samples (i.e., above the vortex annihilation point on the hysteresis loop), in the opposite limit of strong enough applied field. In this situation, the FFA was qualitatively related to the stray fields from unsaturated parts of the magnetization inside the dots.[5] However no quantitative description of this sort of FFA was given up to now. So the present study is aimed at confirming this conjecture and explaining quantitatively this new kind of anisotropy in terms of a modified demagnetizing effect in a patterned planar system at decreasing interdot distance, from the limit of the isolated dot to that of the continuous film. The chosen array geometry permits us to study this effect in the purest form, eliminating other known mechanisms of configurational anisotropy, such as those due to the square form of a dot[10] or the finite size of a square array.[11] The choice of experimental (X-band) FMR techniques has an advantage in eliminating possible interference from domain (vortex) structures.[12] The variational theoretical analysis is followed by micromagnetic simulations.

Permalloy (Py) dots were fabricated with electron beam lithography and lift-off techniques, as explained elsewhere.[13] The dots of thickness $t=50$ nm and diameter $d=1$ μm were arranged into square arrays with the lattice parameter a (center-to-center distance) varying from 1.1 to 2.5 μm. The dimensions were confirmed by atomic force microscopy and scanning electron microscopy. Room-temperature FMR studies were performed at 9.8 GHz using a standard X-band spectrometer. The dependence of the FMR field H_r on the azimuthal angle φ_H of applied field $\mathbf{H}$ with respect to the lattice[10] axis for almost uncoupled dots ($a=2.5$ μm) is shown in Fig. 1(a). Only a weak uniaxial anisotropy of $H_r(\varphi_H)$ is present here, which can be fitted by the simple formula $H_r(\varphi_H)=H_{r,av}+H_2 \cos 2\varphi_H$. For the $a=2.5$ μm sample, we found the average peak position $H_{r,av} \approx 1.13$ kOe and the uniaxial anisotropy field $H_2 \approx 5$ Oe. The latter value remains the same for the rest of our samples, and

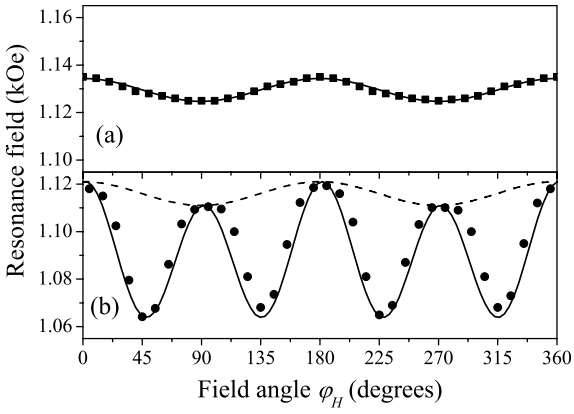

FIG. 1. In-plane FMR field in square lattices of 1 μm circular Py dots as a function of field angle φ_H. (a) The data for lattice parameter $a=2.5$ μm are well fitted by uniaxial anisotropy (solid line). (b) At $a=1.1$ μm, the best fit (solid line) is a superposition of FFA and uniaxial anisotropy (separately shown by dashed line).

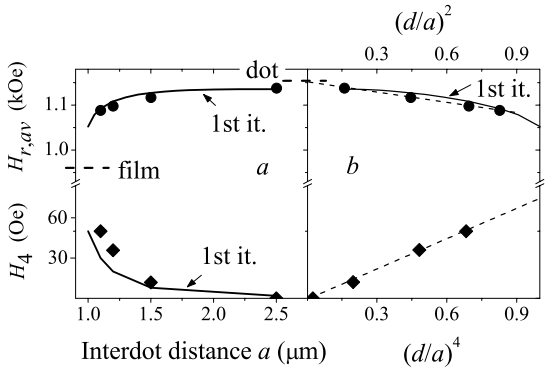

FIG. 2. (a) Average FMR field $H_{r,av}$ and FFA field H_4 as functions of interdot spacing a. The points are the experimental data and the solid lines present the first-iteration theory (the limits mark H_r of an isolated dot and a continuous film). (b) The same data plotted against $(d/a)^2$ for $H_{r,av}$ and $(d/a)^4$ for H_4 give excellent linear fits (dashed lines).

the alignment of this uniaxial anisotropy along one of the lattice axes suggests that it is most probably caused by a slight deviation ($\delta a/a \sim 0.01$) from a square unit cell, by some technological factors.

With decreasing distance a between dots, two changes are observed in the $H_r(\varphi_H)$ dependence. First, $H_{r,av}$ decreases to ≈ 1.09 kOe at $a=1.1$ μm [Fig. 1(b)]. Second, a fourfold anisotropy is detected in the samples with $a \leqslant 1.5$ μm by pronounced minima of $H_r(\varphi_H)$ at φ_H close to the lattice $\langle 11 \rangle$ axes. This behavior is fitted by $H_r(a,\varphi_H)=H_{r,av}(a)+H_4(a)\cos 4\varphi_H+H_2 \cos 2\varphi_H$, as shown in Fig. 1(b). The interdot distance dependence of $H_{r,av}$ and the FFA field H_4 is shown in Fig. 2. Also such anisotropy is detected in the FMR linewidth, smaller for $\langle 11 \rangle$ than for $\langle 10 \rangle$ case (reaching $\sim 30\%$ at $a/d=1.1$).

The FFA effect, which could not arise in uniformly in-plane magnetized cylindrical dots, is evidently related to a nonuniform distribution of the magnetization $\mathbf{m}(r,\varphi,z)$ (in cylindrical coordinates $0 \leqslant r \leqslant R=d/2, 0 \leqslant \varphi < 2\pi, 0 \leqslant z \leqslant t$). In the presence of external fields strong enough to observe FMR, one has to assume a continuous (and mostly slight) deformation of $\mathbf{m}(r,\varphi)$. The simplest model for such deformation used a variational procedure with respect to a single parameter.[14] However, as will be shown below, the nonuniform magnetic ground state of this coupled periodic system results from a rather complicated interplay between intradot and interdot dipolar forces, which requires a more general variational procedure.

Assuming fully planar and z-independent dot magnetization with the two-dimensional (2D) Fourier amplitudes $\mathbf{m}_\mathbf{g}=\int e^{i\mathbf{g}\cdot\mathbf{r}}\mathbf{m}(\mathbf{r})d\mathbf{r}$, the total (Zeeman plus dipolar) magnetic energy (per unit thickness of a dot) can be written as (see the Appendix)

$$E=-\mathbf{H}\cdot\mathbf{m}_0+\frac{2\pi}{a^2}\sum_{\mathbf{g}\neq\mathbf{0}}\frac{f(gt)}{g^2}|\mathbf{m}_\mathbf{g}\cdot\mathbf{g}|^2. \quad (1)$$

Here $f(u)=1-(1-e^{-u})/u$ (Ref. 4) and the vectors of the 2D reciprocal lattice are φ_H dependent: $\mathbf{g}=(2\pi/a)(n_1\cos\varphi_H - n_2\sin\varphi_H, n_1\sin\varphi_H+n_2\cos\varphi_H)$ (for $\mathbf{H}\|x$ and integer $n_{1,2}$). The variation of exchange energy at deformations on the scale of the whole sample is of the order of the stiffness constant ($\sim 10^{-6}$ erg/cm for Py) and it can be neglected compared with the variation $\sim HM_s d^2 \sim 10^{-2}$ erg/cm of terms included in Eq. (1). If the dot magnetization has constant absolute value $\mathbf{m}(\mathbf{r})=M_s(\cos\varphi(\mathbf{r}),\sin\varphi(\mathbf{r}))$, its variation $\delta\mathbf{m}(\mathbf{r})=\hat{\mathbf{z}}\times\mathbf{m}(\mathbf{r})\delta\varphi(\mathbf{r})$ (where $\hat{\mathbf{z}}$ is the unit vector normal to the plane) is due only to the angle variation $\delta\varphi(\mathbf{r})$. Using the Fourier transform $\delta\mathbf{m}_\mathbf{g}=\hat{\mathbf{z}}\times\Sigma_{\mathbf{g}'}\mathbf{m}_{\mathbf{g}-\mathbf{g}'}\delta\varphi_{\mathbf{g}'}$ in the condition $\delta E=0$ leads to the equilibrium equation for the Fourier amplitudes:

$$m_{\mathbf{g},y}=\frac{4\pi}{Ha^2}\sum_{\mathbf{g}'\neq\mathbf{0}}\frac{f(g't)}{g'^2}(\mathbf{m}_{\mathbf{g}'}\cdot\mathbf{g}')(\mathbf{m}_{\mathbf{g}-\mathbf{g}'}\times\mathbf{g}')\cdot\hat{\mathbf{z}}. \quad (2)$$

It can be suitably solved by iterations:

$$m^{(n)}_{\mathbf{g},y}=\frac{4\pi}{Ha^2}\sum_{\mathbf{g}'\neq\mathbf{0}}\frac{f(g't)}{g'^2}(\mathbf{m}^{(n-1)}_{\mathbf{g}'}\cdot\mathbf{g}')(\mathbf{m}^{(n-1)}_{\mathbf{g}-\mathbf{g}'}\times\mathbf{g}')\cdot\hat{\mathbf{z}}, \quad (3)$$

starting from uniformly magnetized dots as the zeroth iteration: $m^{(0)}_{\mathbf{g},y}=0$, $m^{(0)}_{\mathbf{g},x}=2\pi RM_s J_1(gR)/g$ (with the Bessel function J_1). Already the first iteration (including the inverse Fourier transform)

$$m^{(1)}_y(\mathbf{r})=-\theta(d-2r)\frac{8\pi^2R^2M_s^2}{Ha^2}\sum_{\mathbf{g}\neq\mathbf{0}}\frac{f(gt)g_xg_y}{g^3}\times J_1(gR)\cos(\mathbf{g}\cdot\mathbf{r}) \quad (4)$$

(with the Heaviside θ function) reveals the FFA behavior, due to the rotationally noninvariant product g_xg_y. The calculated maximum variation of $\varphi(\mathbf{r})=\arcsin[m_y(\mathbf{r})/M_s]$ in the $\langle 10 \rangle$ field geometry is $\sim 60\%$ bigger than in the $\langle 11 \rangle$ geometry (Fig. 3, top row). Moreover, the two pictures are qualitatively different: the fully "convex" deformation in the $\langle 10 \rangle$ case and the change from central "concave" to peripheral "convex" deformations in the $\langle 11 \rangle$ case reflect the interplay of inter- and intradot dipolar forces. This behavior cannot be obtained with any single variational parameter, and it persists upon further iterations.

Our analytic approach was checked, using the micromagnetic OOMMF code[15] on a 9×9 array of the considered disks (Fig. 3, bottom row) at standard values of $M_s=0.83$ kOe and exchange stiffness $A=1.3\times 10^{-6}$ erg/cm[16] for Py (neglecting its crystalline anisotropy). Each dot was projected onto a 1 μm side square grid of 100×100 elements of 50 nm height. The distributions obtained in this way for the central disk in the array are within $\sim 10\%$ of the analytic results of the first iteration. Practically the same results were obtained setting $A=0$ which confirms the former conclusion on the irrelevant variation of exchange energy in the given system.

The FMR precession of $\mathbf{m}(\mathbf{r})$ is defined by the internal field $\mathbf{H}_i(\mathbf{r})=\mathbf{H}+\mathbf{h}(\mathbf{r})$ through the local dipolar field

$$h_z(\mathbf{r})=-\frac{4\pi}{a^2}\sum_{\mathbf{g}}[1-f(gt)]m_{\mathbf{g},z}\cos(\mathbf{g}\cdot\mathbf{r}),$$

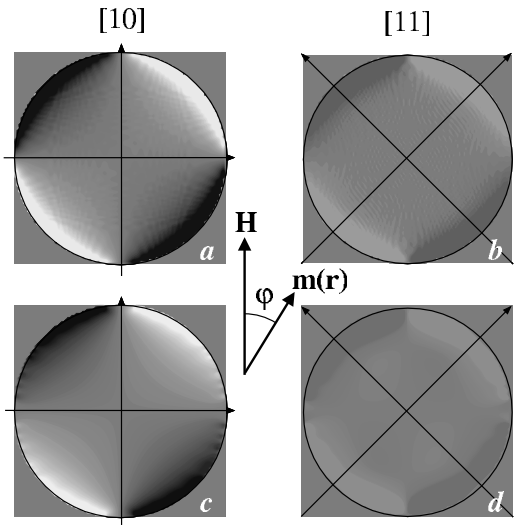

FIG. 3. Density plots of the equilibrium magnetization angle $\varphi(\mathbf{r})$. Top row: calculated from the sum Eq. (4) over 100×100 sites of reciprocal lattice at parameter values $a=1.1$ μm, $H=1.1$ kOe, $M_s=0.83$ kOe, for two field geometries $\varphi_H=$(a) 0 ($\langle10\rangle$) and (b) $\pi/4$ ($\langle11\rangle$). Bottom row: micromagnetic calculation by OOMMF code for the central disk in the 9×9 array for (c) $\langle10\rangle$ and (d) $\langle11\rangle$ geometries.

$$h_\alpha(\mathbf{r}) = -\frac{4\pi}{a^2}\sum_{\beta,\mathbf{g}\neq\mathbf{0}}\frac{f(gt)g_\alpha g_\beta}{g^2}\tilde{m}_{\mathbf{g},\beta}\cos(\mathbf{g}\cdot\mathbf{r}) \tag{5}$$

$(\alpha,\beta=x,y)$. The first iteration for $\mathbf{h}(\mathbf{r})$ corresponds to the zeroth iteration for $\mathbf{m}(\mathbf{r})=(M_s,\mu_y,\mu_z)$, which now includes the uniform FMR amplitudes μ_y,μ_z. Then the local demagnetizing factors $N_x(\mathbf{r})=-h_x(\mathbf{r})/M_s$, $N_{y,z}(\mathbf{r})=-h_{y,z}(\mathbf{r})/\mu_{y,z}$ define the local FMR field $H_r(\mathbf{r})$:

$$H_r(\mathbf{r}) = \sqrt{H_0^2 + M_s^2[N_z(\mathbf{r}) - N_y(\mathbf{r})]^2/4} - M_s[N_z(\mathbf{r}) + N_y(\mathbf{r}) - 2N_x(\mathbf{r})]/2 \tag{6}$$

(here $H_0\approx3.3$ kOe). The average FMR field is defined by the isotropic averaged demagnetizing factors

$$\bar{N}_{x,y} = (\pi R^2)^{-1}\int_{r<R} N_{x,y}(\mathbf{r})d\mathbf{r} = (8\pi^2/a^2)\sum_{\mathbf{g}\neq\mathbf{0}} f(gt)J_1^2(gR)/g^2, \tag{7}$$

and $\bar{N}_z=4\pi-2\bar{N}_x$. At $a\to\infty$, they tend to the single-dot values[17] which are for $t/R=0.1$ $N_{x,y}^{(d)}\approx0.776$ and $N_z^{(d)}\approx11.01$. Using $N_i^{(d)}$ instead of $N_i(\mathbf{r})$ in Eq. (6) accurately reproduces the single-dot FMR limit $H_r^{(d)}\approx1.15$ kOe [estimated from Fig. 2(b)]. Otherwise, for decreasing interdot distance $a\to d$, the first-iteration values Eq. (7) used in Eq. (6) well describe the tendency of $H_{r,av}(a)$ toward the continuous-film limit $H_r^{(f)}=\sqrt{H_0^2+4\pi^2M_s^2}-2\pi M_s\approx0.96$ kOe [Fig. 2(a)].

Finally, by calculating the true local FMR fields $H_r(\mathbf{r})$ from Eqs. (5) and (6), the field-dependent absorption is obtained as $I(H)\propto\int_{r<R}\delta(H-H_r(\mathbf{r}))d\mathbf{r}$. Then the FMR fields H_r defined from the maximum of $I(H)$ in two geometries display FFA in good agreement with the experimental data (Fig. 2). This effect is due to the fact that stronger deformation of magnetization more strongly suppresses the demagnetizing effect (the differences $N_z-N_{x,y}$) and thus enhances H_r. Also it produces a bigger spread of local resonance fields $H_r(\mathbf{r})$ and thus broadens the FMR line, again in agreement with our observations.

In conclusion, it is shown that under in-plane magnetic fields $\mathbf{H}$ even strong enough for FMR, the dipolar coupling in a dense lattice of circular magnetic dots is able to produce a continuous deformation of the dot magnetization, strongest for the field orientation along lattice axes, leading to a specific fourfold anisotropy. The possible effect of weak uniaxial (magnetocrystalline) anisotropy should be less sensitive to this deformation and can be simply added to it [as in Fig. 1(b)].

Work at ANL was supported by the U.S. Department of Energy, BES Materials Sciences under Contract No. W-31-109-ENG-38; M.D.C. was supported by FCT (Portugal) and the European Union, through POCTI (QCA III) Grant No. SFRH/BD/7003/2001.

APPENDIX

For fully planar and z-independent dot magnetization, the dipolar energy per unit thickness of a dot in the lattice is

$$E_d = \frac{1}{2t}\int_{-t/2}^{t/2}dz\int_{-t/2}^{t/2}dz'\int_c d\mathbf{r}\int d\mathbf{r}'\sum_{\alpha,\beta}m_\alpha(\mathbf{r}) \times\frac{\partial^2}{\partial r_\alpha\partial r_\beta}\frac{m_\beta(\mathbf{r}')}{\sqrt{|\mathbf{r}-\mathbf{r}'|^2+(z-z')^2}},$$

where the 2D integrations $\int_c d\mathbf{r}$ and $\int d\mathbf{r}$ are, respectively, over the unit cell and over the entire plane. It can also be presented as

$$E_d = \frac{1}{2t}\int_{-t/2}^{t/2}dz\int_c d\mathbf{r}\sum_\alpha m_\alpha(\mathbf{r})h_a(\mathbf{r},z) = \frac{1}{4\pi ta^2}\int_{-t/2}^{t/2}dz\int_{-\infty}^{\infty}dq\,e^{-iqz}\sum_{\alpha,\mathbf{g}}m_{\alpha,\mathbf{g}}h_{\alpha,\mathbf{g},q},$$

where the Fourier amplitudes of the dipolar field are

$$h_{\alpha,\mathbf{g},q} = \int_c d\mathbf{r}\int_{-\infty}^{\infty}dz\,e^{i(\mathbf{g}\cdot\mathbf{r}+qz)}h_a(\mathbf{r},z) = \int_c d\mathbf{r}\int_{-\infty}^{\infty}dz\,e^{i(\mathbf{g}\cdot\mathbf{r}+qz)}\int d\mathbf{r}'\int_{-t/2}^{t/2}dz' \times\sum_\beta\frac{\partial^2}{\partial r_\alpha\partial r_\beta}\frac{m_\beta(\mathbf{r}')}{\sqrt{|\mathbf{r}-\mathbf{r}'|^2+(z-z')^2}}.$$

Then we express $m_\beta(\mathbf{r}')$ through its Fourier amplitudes:

$$m_\beta(\mathbf{r}') = \frac{1}{a^2}\sum_{\mathbf{g}'}e^{-i\mathbf{g}'\cdot\mathbf{r}'}m_{\beta,\mathbf{g}'},$$

and introduce the factor $e^{i(\mathbf{g}'\cdot\mathbf{r}-qz')}$ into the integral in $d\mathbf{r}'dz$, and the compensating factor $e^{-i(\mathbf{g}'\cdot\mathbf{r}-qz')}$ into the integral in

$d\mathbf{r}\, dz'$. Then the spatial integrations in E_d are done according to the formulas

$$\int_c d\mathbf{r}\, e^{i(\mathbf{g}-\mathbf{g}')\cdot\mathbf{r}} = a^2 \delta_{\mathbf{g},\mathbf{g}'},$$

$$\int_{-t/2}^{t/2} dz \int_{-t/2}^{t/2} dz' e^{iq(z'-z)} = \frac{4}{q^2} \sin^2 \frac{qt}{2},$$

$$\int_{-\infty}^{\infty} dz' \int d\mathbf{r}' e^{i\mathbf{g}\cdot(\mathbf{r}-\mathbf{r}')+iq(z-z')} \frac{\partial^2}{\partial r_\alpha \partial r_\beta} \frac{1}{\sqrt{|\mathbf{r}-\mathbf{r}'|^2+(z-z')^2}} = \frac{4\pi g_\alpha g_\beta}{g^2+q^2}.$$

Finally, the momentum integration

$$\int_{-\infty}^{\infty} \frac{\sin^2(qt/2)}{q^2(g^2+q^2)} dq = \frac{\pi t}{2g^2} f(gt)$$

leads to the result of Eq. (1).

[1] A. Moser, K. Takano, D. T. Margulies, M. Albrecht, Y. Sonobe, Y. Ikeda, S. Sun, and E. E. Fullerton, J. Phys. D **35**, R157 (2002); S. Sun and D. Weller, J. Magn. Soc. Jpn. **25**, 1434 (2001).

[2] D. A. Allwood, Gang Xiong, M. D. Cooke, C. C. Faulkner, D. Atkinson, N. Vernier, and R. P. Cowburn, Science **296**, 2003 (2002).

[3] S. O. Demokritov, B. Hillebrands, and A. N. Slavin, Phys. Rep. **348**, 441 (2001).

[4] K. Yu. Guslienko and A. N. Slavin, J. Appl. Phys. **87**, 6337 (2000); J. Magn. Magn. Mater. **215**, 576 (2000).

[5] C. Mathieu, C. Hartmann, M. Bauer, O. Büttner, S. Riedling, B. Roos, S. O. Demokritov, and B. Hillebrands, Appl. Phys. Lett. **70**, 2912 (1997).

[6] S. Jung, B. Watkins, L. DeLong, J. B. Ketterson, and V. Chandrasekhar, Phys. Rev. B **66**, 132401 (2002).

[7] M. Natali, A. Lebib, Y. Chen, I. L. Prejbeanu, and K. Ounadjela, J. Appl. Phys. **91**, 7041 (2002).

[8] X. Zhu, P. Grutter, V. Metlushko, and B. Ilic, Appl. Phys. Lett. **80**, 4789 (2002).

[9] K. Yu. Guslienko, Phys. Lett. A **278**, 293 (2001).

[10] R. P. Cowburn, A. O. Adeyeye, and M. E. Welland, Phys. Rev. Lett. **81**, 5414 (1998).

[11] Yu. B. Grebenschikov, N. A. Usov, and K. Yu. Guslienko, Mater. Sci. Forum **373-376**, 149 (2001).

[12] G. N. Kakazei, P. E. Wigen, K. Y. Guslienko, R. W. Chantrell, N. A. Lesnik, V. Metlushko, H. Shima, K. Fukamichi, Y. Otani, and V. Novosad, J. Appl. Phys. **93**, 8418 (2003).

[13] V. Novosad, K. Yu. Guslienko, H. Shima, Y. Otani, S. G. Kim, K. Fukamichi, N. Kikuchi, O. Kitakami, and Y. Shimada, Phys. Rev. B **65**, 060402(R) (2002).

[14] K. L. Metlov, Phys. Status Solidi A **189**, 1015 (2002); K. L. Metlov and K. Yu. Guslienko, Phys. Rev. B **70**, 052406 (2004).

[15] M. J. Donahue and D. G. Porter, URL: http://math.nist.gov/oommf

[16] G. N. Kakazei, P. E. Wigen, K. Y. Guslienko, V. Novosad, A. N. Slavin, V. O. Golub, N. A. Lesnik, and Y. Otani, Appl. Phys. Lett. **85**, 443 (2004).

[17] R. I. Joseph and E. Schlömann, J. Appl. Phys. **36**, 1579 (1965).